

Andrew Duenner

Department of Mechanical Engineering,
University of Texas at Austin,
Austin, TX 78712

Tsung-Fu Yao

Department of Mechanical Engineering,
University of Texas at Austin,
Austin, TX 78712

Bruno De Hoyos

Department of Mechanical Engineering,
University of Texas at Austin,
Austin, TX 78712

Marianna Gonzales

Department of Mechanical Engineering,
University of Texas at Austin,
Austin, TX 78712

Nathan Riojas

Department of Mechanical Engineering,
University of Texas at Austin,
Austin, TX 78712

Michael Cullinan

Department of Mechanical Engineering,
University of Texas at Austin,
Austin, TX 78712

A Low-Cost, Automated Wafer Loading System With Submicron Alignment Accuracy for Nanomanufacturing and Nanometrology Applications

This paper introduces a low-cost, automated wafer alignment system capable of submicron wafer positioning repeatability. Accurate wafer alignment is critical in a number of nanomanufacturing and nanometrology applications where it is necessary to be able to overlay patterns between fabrication steps or measure the same spot on a wafer over and over again throughout the manufacturing process. The system presented in this paper was designed to support high-throughput nanoscale metrology where the goal is to be able to rapidly and consistently measure the same features on all the wafers in a wafer carrier without the need for slow and expensive vision-based alignment systems to find and measure the desired features. The wafer alignment system demonstrated in this paper consists of a three-pin passive wafer alignment stage, a voice coil actuated nesting force applicator, a three degrees-of-freedom (DOFs) wafer handling robot, and a wafer cassette. In this system, the wafer handling robot takes a wafer from the wafer cassette and loads it on to the wafer alignment stage. The voice coil actuator is then used to load the wafer against the three pins in the wafer alignment system and align the wafer to an atomic force microscope (AFM)-based metrology system. This simple system is able to achieve a throughput of 60 wafers/h with a positional alignment repeatability of 283 nm in the x-direction, 530 nm in the y-direction, and 398 nm in the z-direction for a total capital cost of less than \$1800. [DOI: 10.1115/1.4034610]

1 Introduction

In a typical semiconductor manufacturing setting, wafers are transported in cassettes by guided vehicles and loaded into or unloaded from machines by wafer handling robots [1]. The critical dimension of features patterned in modern semiconductor manufacturing processes continues to decrease without a significant impact on manufacturing throughput. As a result, a gap is emerging in the field of semiconductor metrology where few technologies are capable of in-line metrology. Recent advances in microelectromechanical systems (MEMS) fabrication have enabled the realization of an entire AFM on a single MEMS chip. This MEMS-based AFM is capable of high-speed scanning of nanoscale features over micron scale areas and is small enough that it can be incorporated into manufacturing tools for in situ nanoscale measurements or into metrology platforms with multiple scanning probes operating on a wafer at the same time [2]. These low-cost devices dramatically reduce setup time required for AFM metrology due to the fact that they do not require the focusing of a laser on an AFM cantilever tip as is common with traditional AFM systems and do not require the inspection wafer to be loaded into a large AFM system where it is necessary to search for the spot on the wafer the user wants to inspect before a measurement can be made. Improvements in the scanning area and throughput are made possible by the MEMS-based AFMs through the incorporation of multiple AFM chips on a platform as described in Ref. [3]. The system described in this paper aims to further reduce the setup time of AFM-based metrology by enabling the repeatable alignment of wafers into a low cost, AFM-

based metrology system in order to realize the ultimate goal of high-throughput AFM-based nanoscale metrology of semiconductor wafers.

This type of metrology system would enable in-line metrology of silicon wafers after a lithography or etching step in the semiconductor manufacturing process. Currently, it is not possible to measure nanoscale features in-line with the semiconductor manufacturing process since most nanoscale metrology methods are too slow for in-line process measurements [4]. Therefore, in semiconductor manufacturing processes, a few wafers are taken off the manufacturing line each hour and inspected using time-intensive methods such as scanning electron microscopy. This means that many defective wafers can travel through the manufacturing process before an error is detected. In-line metrology enabled by the precision alignment methods described in this paper will help to detect these errors much quicker in the manufacturing process and reduce the scrap rate in semiconductor manufacturing.

2 Background

Transport of wafers between semiconductor manufacturing equipment is typically accomplished by wafer handling robots. Typical wafer handling robots are based on the selective compliance arm for robot assembly (SCARA) robot platform [5]. SCARA wafer handling robots commonly operate in a horizontal work plane with 1DOF in the vertical direction and 3DOF in the horizontal plane [5]. These wafer handling robots are typically capable of throughputs of up to 350 wafers/h and positioning repeatability on the order of 100 μm [6,7].

Coarse optical alignment of wafers is often achieved by rotating the wafer and using an optical sensor to determine the location of the wafer flat [8]. Wafers can be precisely aligned with respect to

Contributed by the Manufacturing Engineering Division of ASME for publication in the JOURNAL OF MICRO- AND NANO-MANUFACTURING. Manuscript received June 12, 2016; final manuscript received September 1, 2016; published online October 10, 2016. Assoc. Editor: Rajiv Malhotra.

a metrology tool either by active or passive means. Active wafer alignment is typically achieved by optical means. The most common method of optical wafer alignment involves patterning alignment marks onto a wafer substrate [8]. These alignment marks are viewed under a microscope containing a matching mark. Alignment is achieved when the two marks are in line with each other. Submicron repeatability has been demonstrated using this method [9,10]. Manual wafer registration via optical alignment is a time-intensive process that is not practical for in-line metrology applications. Automated optical alignment systems that use robotic arms and vision systems to achieve submicron wafer alignment have been demonstrated, but it is very expensive to implement these alignment systems in metrology systems that do not already have imaging optics and closed-loop controls for wafer placement. Such robotic, vision-based wafer alignment systems can cost upward of \$100,000. More advanced optical alignment systems also exist that rely on interference patterns from moiré marks and are capable of sub-20 nm wafer alignment [11]. However, these systems are typically only implemented in multimillion dollar nanomanufacturing tools that require extremely good wafer alignment repeatability since their cost and resolution are much greater than required for a general purpose semiconductor metrology platform.

Passive wafer alignment is a desirable alternative to active optical alignment in metrology systems requiring high throughput, repeatability better than $1\ \mu\text{m}$, and low cost of integration since passive alignment systems are capable of submicron repeatabilities but do not require the expensive vision and control systems commonly found in active alignment systems. For example, Slocum and Weber demonstrated the ability to achieve submicron repeatability in wafer alignment [12] through the fabrication of microstructures on wafers that take advantage of the principle of elastic averaging [13]. However, in many cases, it is expensive and undesirable to add any features to a wafer for the purposes of metrology. Passive alignment based on pin constraints is a low-cost wafer alignment method that, through proper design and implementation, is capable of achieving micron scale alignment repeatabilities [14]. In this mode of wafer alignment, wafers are exactly constrained [15] by three pins in the XY plane, as shown in Fig. 1. Two of the pins are on the flat of the wafer and a third pin is strategically located on the diameter. A preload force maintains contact between the wafer and the pins and allows the wafer to self-align with the stage. Passive alignment has shown promising results for repeatability on the order of $2\ \mu\text{m}$ [14]. However, such passive alignment systems are commonly manually loaded, which results in low throughput and alignment repeatability that is

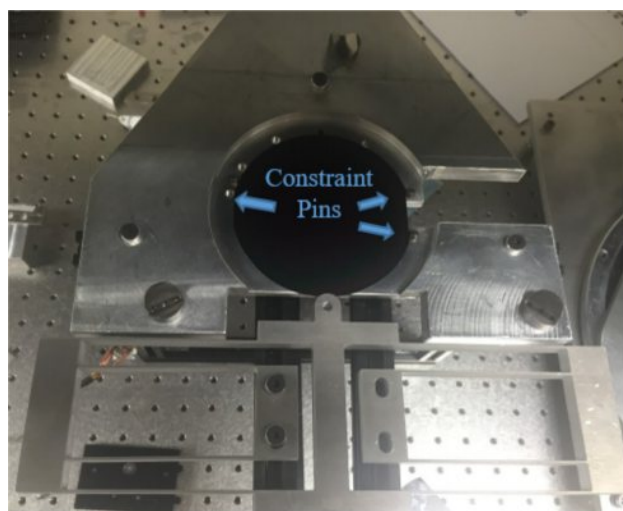


Fig. 1 Arrangement of three constrain pins in passive wafer alignment system

dependent on the human user. The system described in this paper aims to improve both the repeatability and the throughput of passive wafer alignment systems in order to support true in-line wafer metrology for nanomanufacturing applications. The overall goal of this work is to demonstrate that through the use of passive alignment systems in combination with a low-cost wafer handling system, wafer alignment repeatabilities can be achieved that are competitive with state-of-the-art robotic wafer handling arms at a fraction of the cost.

3 Design

3.1 Theory of Operation. The automated wafer handling system consists of a number of components including a passive wafer alignment stage, a wafer handling robot, and a standard wafer cassette. In this system, the wafer handling robot is used to pick up a wafer from the wafer cassette and place it onto the alignment platform. The wafer handling robot utilizes a vacuum chuck to systematically grip or release wafers from the bottom surface in order to prevent damage to the patterned top surface. On the wafer alignment platform, three pins are used to align the wafer on the inspection stage. Two of the pins are loaded against the flat on the wafer and one pin is placed at the optimal location to maximize the nesting force on the wafer [14]. A voice coil-driven flexure mechanism is then automatically engaged and used to push the wafer up against the three alignment pins in the system. Once the wafer has been loaded into the system, the metrology frame or AFM system can then be placed onto the inspection stage using a set of kinematic couplings in order to take a measurement of the wafer alignment accuracy or to measure features on the surface of the wafer. These kinematic couplings were measured to have a repeatability of 390 nm, 361 nm, and 60.0 nm in the X, Y, and Z directions, respectively [3]. Once the measurement on the wafer has been completed, the metrology frame/AFM system can be removed from the system and the wafer handling robot can be used to remove the wafer from the system and return it to the wafer cassette. The wafer handling robot can then be used to pick up the next wafer from the wafer cassette and the process can be repeated until all 25 wafers in the cassette have been measured. The wafer alignment system and wafer handling robot system are controlled by an operator via a LABVIEW-based program and a National Instruments MyRIO that allows wafers to be loaded or unloaded from a passive alignment mechanism into one of the slots in the wafer cassette. The loading program utilizes preconfigured “recipes” to load and unload wafers based on the initial position of the wafers within the wafer carrier and the relative locations of the wafer carrier and the alignment/metrology stage. A diagram of the major system components is shown below in Figs. 2 and 3 shows the flow chart of loading/unloading procedures in operation.

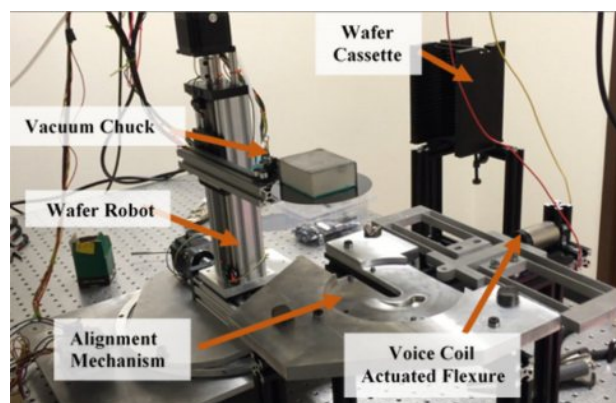


Fig. 2 Wafer alignment system

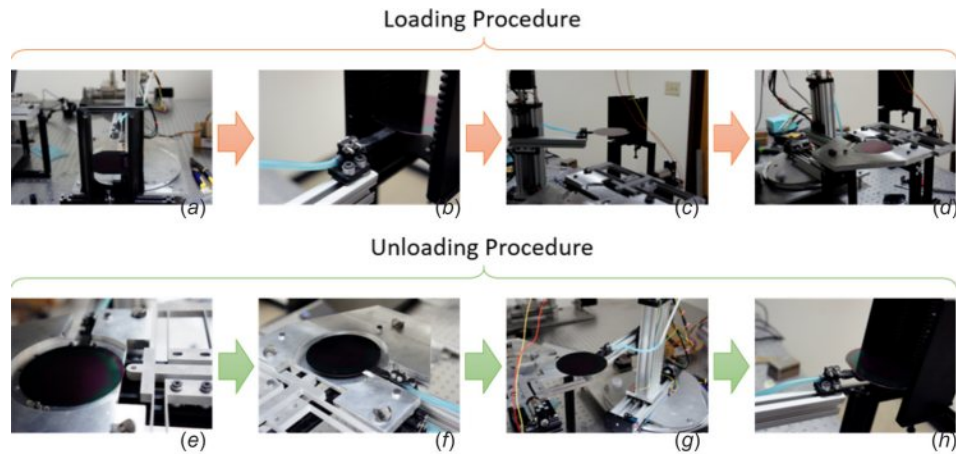


Fig. 3 Flowchart of loading operation: (a) wafer in cassette, (b) handling system grabs wafer, (c) wafer transportation, (d) wafer release and flexure preload to put into alignment mechanism, and unloading operation (e) flexure release, (f) handling system grabs wafer, (g) wafer transportation, and (h) back to cassette

3.2 Wafer Handling Robot. The automated wafer handling system operates in a cylindrical workspace with one rotational axis and two translational axes. The cylindrical coordinate system was chosen to minimize the footprint of the wafer handling robot as well as the number of actuated DOFs. The serial configuration of the axes requires that the axis connected to the ground have relatively low errors since any errors in this axis will propagate to the other axes. In order to meet this requirement, a rotational stage driven by a stepper motor was chosen for the axes connected to ground. The rotational stage is connected to the stepper motor using a timing belt with a 4:1 reduction ratio. A low-cost “lazy-Susan” turntable was utilized as a bearing to handle both the radial loads of the tensioned timing belt and the axial load exerted by the base plate and linear axes. The turntable consists of an inner and outer raceway with spherical steel balls separating the two cast aluminum raceways. The balls in the turntable provide low resistance to rotation of the stage and the turntable is rated to support substantial axial loads. The repeatability of the turntable was tested under load conditions to verify that its error motion was sufficiently low to meet the repeatability requirements of the system. This design for the rotational axis helps to reduce manufacturing cost while still maintaining the required level of precision. A computer-aided design (CAD) model of the rotary axis is shown in Fig. 4.

The two translational axes are stacked in series on top of the rotary platform fixed to the outer raceway of the turntable bearing. One axis translates radially with respect to the rotating axis and the other axis (stacked on top of the radial axis) translates in an

axial direction with respect to the rotating axis. Each translational axis consists of a carriage with four wheels sliding on an extruded aluminum rail. Eccentric nuts on two of the wheels are used to apply a preload to the wheels and increase the out-of-plane stiffness of the linear axes. The carriages on each linear axis are connected to lead screws by antbacklash nuts that minimize the hysteresis in the lead screw motion. A CAD rendering of the entire system is shown in Fig. 5.

Stepper motors were selected to drive all of the axes because they allow for precise motion control in an open loop control configuration. In order to determine the size of stepper motor required, torque and speed requirements were calculated for each axis. Speed requirements were based on the assumption that every axis is allocated 5 s of travel time in order to meet the desired wafer throughput target of 60 wafers/h. Trapezoidal velocity profiles were constructed such that 20% of travel time was allocated to acceleration, 60% was allocated to constant velocity travel, and 20% of travel time was allocated to deceleration.

The rotary axis torque requirements were driven by the torque required to overcome friction and the torque required to accelerate the turntable. A conservative estimate of 10 kg was made for rotating mass, and the radius of the rotating element was estimated to be 105 mm corresponding to the radius of the turntable. The coefficient of friction of the turntable bearing was estimated to be 0.0015, which is a typical value for ball bearings [16]. Rotational inertia was then calculated using Eq. (1), where m and r are the mass and radius of the stage

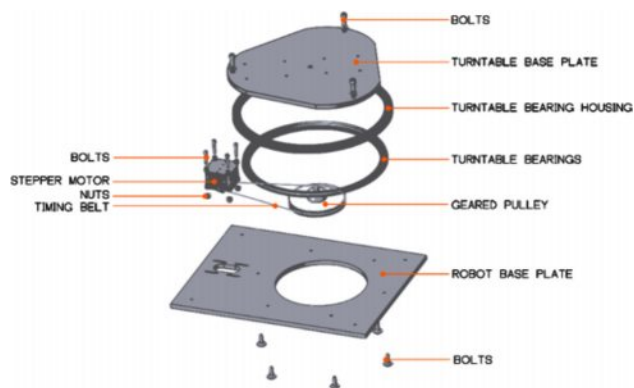


Fig. 4 Rotary axis exploded view

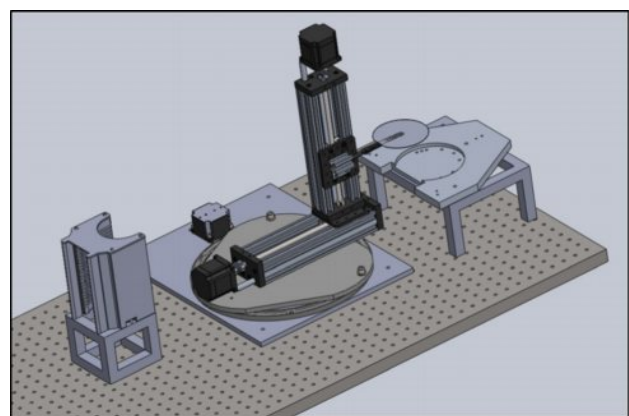


Fig. 5 CAD rendering of wafer handling robot

$$J = \frac{1}{2}mr^2 \quad (1)$$

Using this equation, the rotational inertia of the stage was calculated to be 0.116 kg/m². The mass on the turntable bearings was assumed to be a uniform cylinder, as shown in the free-body diagram in Fig. 6. Torque required to accelerate the turntable, τ_a , was calculated as the rotational moment of inertia of the turntable multiplied by the angular acceleration as shown in Eq. (2), where α is the angular acceleration

$$\tau_a = J\alpha \quad (2)$$

The trapezoidal velocity profile was used to determine the maximum rotational velocity and acceleration values. For this velocity profile, the travel distance is given by Eq. (3) where the maximum rotational velocity is ω_{\max} , the acceleration time is t_a , and the total time is t_f

$$\theta = (t_f - t_a)\omega_{\max} \quad (3)$$

Solving for ω_{\max} given that $\theta = \pi$ radians for the velocity profile selected yields a maximum rotational velocity of $\pi/4$ rad/s. Achieving this angular velocity in 1 s requires an acceleration of $\pi/4$ rad/s². Thus, the torque requirement for the rotary axis acceleration is 0.091 N-m. Friction to overcome torque is found from Eq. (4), where μ is the coefficient of friction and g is gravity

$$\tau_f = \mu * m * g * r \quad (4)$$

For the turntable bearing radius of 150 mm, the estimated friction torque is 0.022 N-m. In order to better match the torque and speed requirements to that of commonly available stepper motors, a 4:1 pulley radius ratio was selected with the smaller pulley attached to the stepper motor. This reduces torque requirement for the stepper motor to 0.028 N-m or 25% of the torque required to turn the turntable. Similarly, this pulley ratio increases the speed requirement of the stepper motor to 400% of the turntable requirement or 3.14 rad/s.

Typical stepper motors are capable of 200 steps per revolution or 1.8 deg/step. Therefore, an angular velocity of 3.14 rad/s corresponds with a frequency of 100 Hz for full stepping and 200 Hz for half stepping. A design safety factor of four was applied to the torque requirement in order to yield a design torque of 0.112 N-m or approximately 16 oz-in at a frequency of 200 Hz.

Calculations for each of the translational axes were made in a similar fashion. Force requirements for friction and acceleration were determined and converted to leadscrew torque. Maximum acceleration required to translate 200 mm in 5 s with a trapezoidal profile yielded an acceleration requirement of 0.05 m/s². Multiplying by a conservative moving mass estimate of 10 kg results in a total thrust force requirement of 0.5 N. The friction coefficient for wheels on rails was estimated to be 0.01 [13] and the total friction

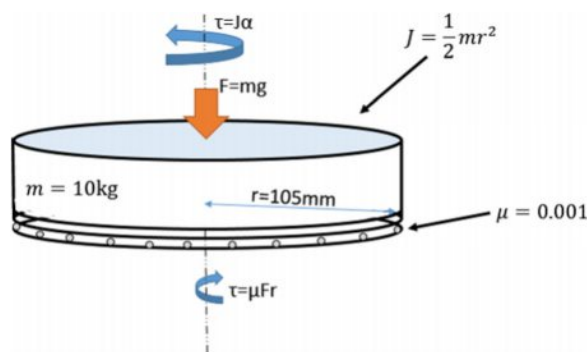


Fig. 6 Free-body diagram for turntable calculations

force was estimated to be 0.98 N. The equation for converting lead screw force to torque is shown in Eq. (5) with acceleration force, F , coefficient of friction between nut and screw, μ , pitch diameter, d_p , lead distance, L , and thread angle, α [16]

$$T = \frac{Fd_p(\mu\pi d_p + L \cos \alpha)}{2(\pi d_p \cos \alpha + \mu L)} \quad (5)$$

The leadscrew selected for the first iteration of analysis was 8 mm in diameter with a pitch of 2 mm and a lead of 8 mm. The thread angle for acme threads is 14.5 deg [16] and a conservative friction coefficient of 0.1 was estimated for the friction between the screw and the plastic nut. The resulting torque requirement was estimated to be 5.3 N-mm or 0.72 oz-in. The stepping speed requirement was determined by converting the required velocity of 0.05 m/s to an angular velocity using the lead of the leadscrew. The required angular velocity is then 6.25 revolutions per second or 1250 Hz for a standard half-stepping stepper motor. With microstepping, it was found that a maximum of 800 steps per revolution was technically achievable, which would result in translational positioning resolution on the order of 10 μ m.

4 Error Budget

The data characterizing performance of critical machine elements used in the wafer loading mechanism such as bearings and linear motion stages is difficult to estimate from theory. Therefore, the repeatability of each axis was measured independently and utilized to estimate an error budget for the repeatability of the entire system. A capacitance probe fixture, shown in Fig. 7, was utilized to characterize the repeatability of both of the axes.

Coordinate frames were constructed for each moving axis as shown in Fig. 8 and homogeneous transformation matrices (HTM) were used to translate the tool tip (vacuum wand) from the starting position in the wafer cassette to a finishing position at the wafer loading stage. Starting with the tool tip coordinate system, translational transformations take the form shown in Eq. (6) [13] with rotational errors represented by the epsilon terms and the subscript of each term indicating the axis about which the rotation occurs

$${}^R T_N = \begin{bmatrix} 1 & -\epsilon_z & \epsilon_y & a + \delta_x \\ \epsilon_z & 1 & -\epsilon_x & b + \delta_y \\ -\epsilon_y & \epsilon_x & 1 & c + \delta_z \\ 0 & 0 & 0 & 1 \end{bmatrix} \quad (6)$$

Large translations are represented by a , b , and c terms and translational error motions are represented by the delta terms with the subscript indicating the direction of the error motion. The transformation matrix for a rotary axis takes the form shown in the below equation [13]

$${}^R T_N = \begin{bmatrix} \cos \theta_z & -\sin \theta_z & \epsilon_y & \delta_x \\ \sin \theta_z & \cos \theta_z & -\epsilon_x & \delta_y \\ \epsilon_x \sin \theta_z - \epsilon_y \cos \theta_z & \epsilon_x \cos \theta_z + \epsilon_y \sin \theta_z & 1 & \delta_z \\ 0 & 0 & 0 & 1 \end{bmatrix} \quad (7)$$

The 1- σ repeatability values for each actuated axis were used as error terms. After determining the transformation from the tool tip to the reference coordinate frame, the transformation from the work surface (wafer) to the reference frame was calculated. The relative error in the reference coordinate system was calculated by taking the cross product of the inverse of the tool-tip HTM and the workpiece HTM [13]. The calculated position error from this error budget is shown in Table 1 and compared to the actual measured results.

Table 1 shows the comparison of combined random error between predicted and measured values. Overall, the calculated error budget produces result that overestimate the error in the

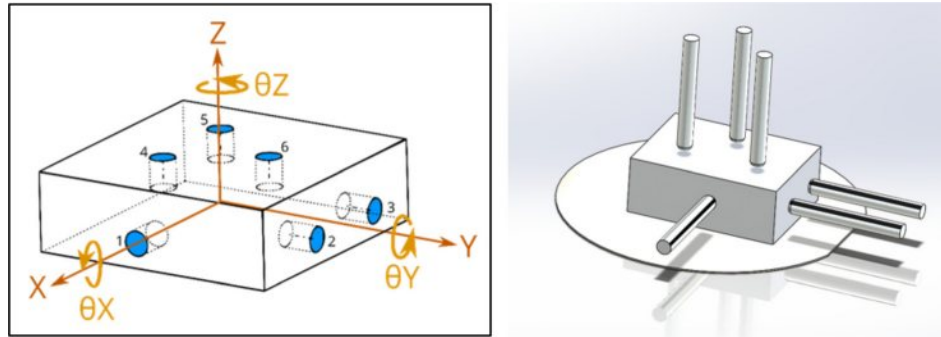


Fig. 7 (Left) Measurement spots (1–6) for capacitance probes on reference block showing coordinate axis of the measurements and (right) schematic of capacitance probe setup relative to the measurement block and the wafer that is loaded into the system

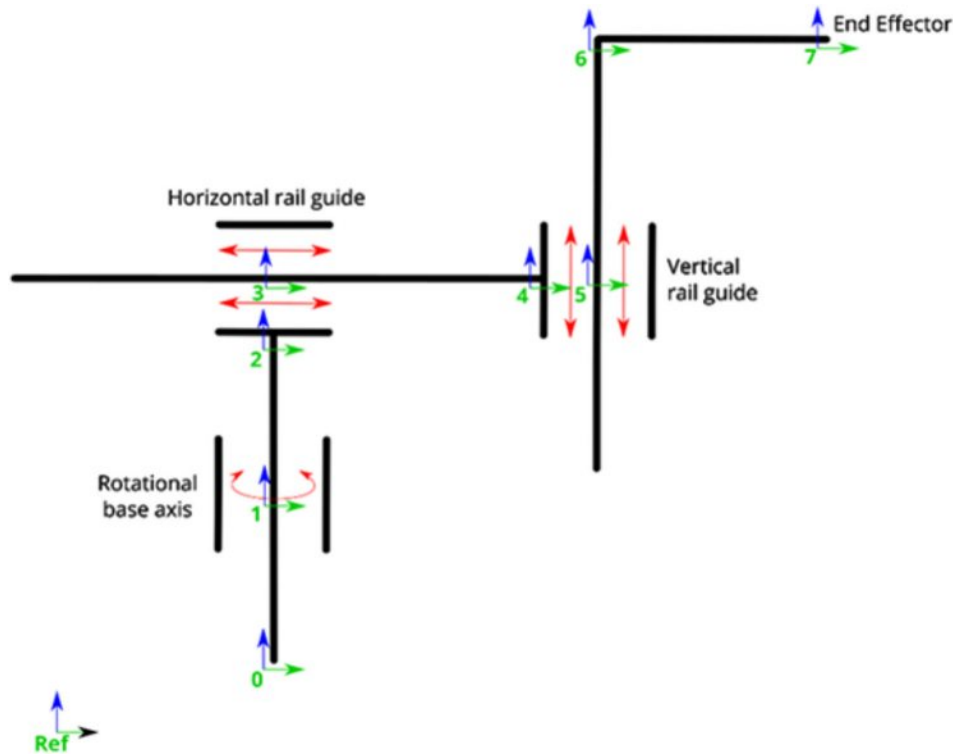


Fig. 8 Error budget coordinate frames

system compared to the measured combined repeatability error of the wafer handling system. This is most likely due to the fact that very conservative estimates were made about the error sources in both the controls and the mechanical components of the system. The model is most sensitive to rotational errors about the x - and y -axes of both the rotating platform and the translating x -axis. Future system improvements will focus on improving rotational repeatability in these sensitive axes that are identified by this model of the system.

Table 1 Combined random error predicted versus measured

	Translation (μm)			Rotation (mrad)		
	X	Y	Z	θ_x	θ_y	θ_z
Predicted	107.0	35.0	85.0	0.347	1.10	0.346
Actual	9.8	5.2	5.4	0.139	0.469	0.518

5 Results

Testing of the wafer loading mechanism was performed to determine the overall repeatability of the system. A capacitance probe fixture was designed to couple with the alignment stage via kinematic couplings (Fig. 9). The probe fixture was used to record displacements of the probes relative to a conductive element bonded to the top surface of a wafer. Initial setup of the testing procedure required that the wafer be manually placed in the alignment stage. For each subsequent test, the wafer loading robot was commanded to unload the wafer from the alignment stage, place the wafer into a slot in the wafer cassette, remove the wafer from the cassette, and finally place the wafer back into the wafer alignment stage. The capacitance probe metrology frame was then coupled to the alignment stage using the kinematic coupling mounts to measure displacement relative to the first trial. The results from the repeatability tests were characterized by a nonuniform distribution with approximately 90% of the trials indicating submicron repeatability and 10% of trials visibly misaligned with the pins on the alignment stage. Figure 10 shows

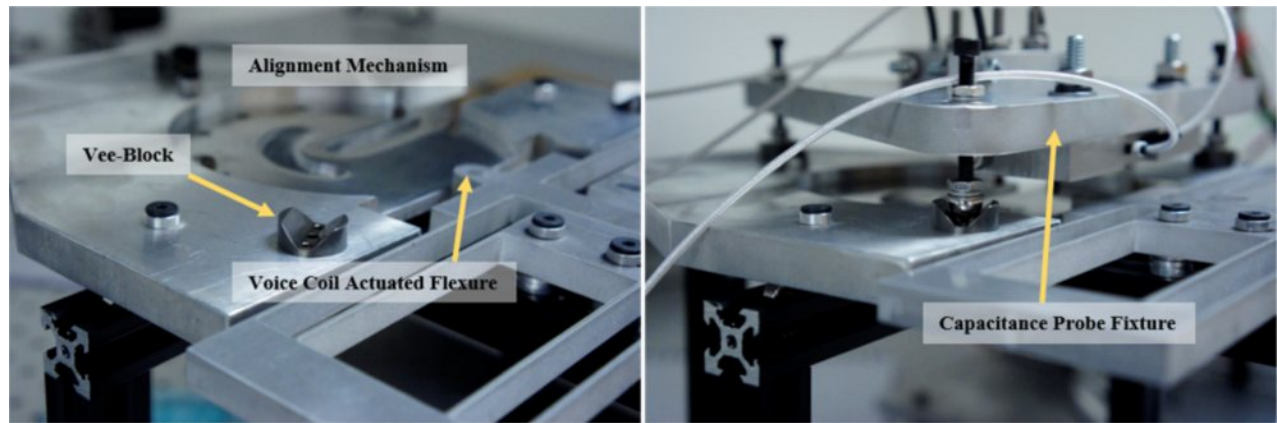


Fig. 9 (Left) Kinematic coupling consists of a Vee-block and truncated ball ensuring position repeatability between capacitance probe fixture and alignment mechanism (right) capacitance probe fixture in use

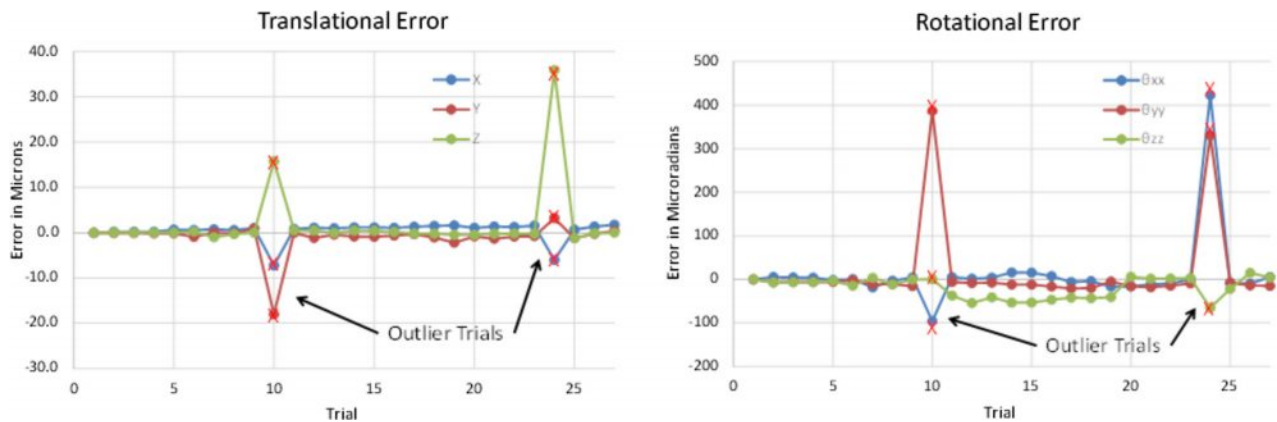


Fig. 10 (Left) Translational and (right) rotational error distribution with outliers

the loading of 25 wafers from a standard wafer carrier. Outliers are represented by red X marks and are indicative of trials with wafer placement error that is outside the 99% confidence error of the trials. These outliers are caused by the wafer not becoming fully engaged with the three-pin passive alignment system. This can happen when the wafer is loaded at an angle causing one of the two pins that create the constraint in the y direction to not come in contact with the wafer flat. If the actuator force is not enough to overcome friction, or if the wafer is too far away from the three pins, the wafer alignment system will not properly align the wafers. However, these errors generally self-correct as evidenced in Fig. 8 as reloading the wafer again. The loading error returns to its nominal level without making any changes to the system. This suggests that relatively minor random errors in the loading system can create significant wafer alignment errors if these random errors cause the initial wafer loading position to be outside the capture area of the wafer three-pin alignment system. Therefore, in the wafer testing procedure, if one wafer loading is found to be outside the capture area of the three-pin alignment system, the loading of that wafer is repeated in order to eliminate outliers from the loading of the complete 25 wafer set. Overall, about 10% of the wafer loadings resulted in these types of alignment outliers.

In order to detect these outliers, a low-cost, knife-edge sensor can be implemented to detect large wafer misalignments and to determine if the wafer needs to be reloaded into the system. As such, outlier error values greater than the expected misalignment detection resolution of $10\ \mu\text{m}$ were omitted from the repeatability results shown in Fig. 11. These figures indicate that the wafer

loading system is capable of submicron repeatability over 25 wafers or roughly the number of wafers that would be loaded into a cassette. Overall, there is some drift in the wafer loading over time with the final center position of the last wafer loaded into the system being about $1.8\ \mu\text{m}$ off from the initial position of the first wafer. Less drift is observed in the rotational error but trials 11–18 show significantly more rotational error around the z-axis than the other trials. This could have been caused by a particle sticking to one of the pins on the wafer stage on the 11th trial and falling off by the 18th trial. The total in-plane (lateral) translational error measured as the standard deviation from average center point of the wafer over the 25 trials after the outlier points were removed was measured to be $634\ \text{nm}$. The total in-plane (θ_z) rotational error of the wafer loading was measured to be $22.8\ \mu\text{rad}$.

Table 2 shows the standard deviation of wafer placement errors over 25 wafers. These total error measurements, however, overestimate the error in the wafer loading because the metrology frame is not fixed. Between each wafer loading operation, the metrology frame holding the capacitance probes is removed from the system and placed back into the system using a set of kinematic couplings. Therefore, since the kinematic couplings are not perfectly repeatable, the measured error is a combination of the wafer loading error and the error in the kinematic couplings. Assuming that errors in the wafer loading and the kinematic coupling are random and uncorrelated, we can estimate the error in just the loading of the wafer without the stacked error of the measurement system due to the uncertainty in the kinematic coupling using Eq. (8) where σ_{Wafer} is the standard deviation of the wafer position, σ_{Measured} is the actual measured standard deviation of the

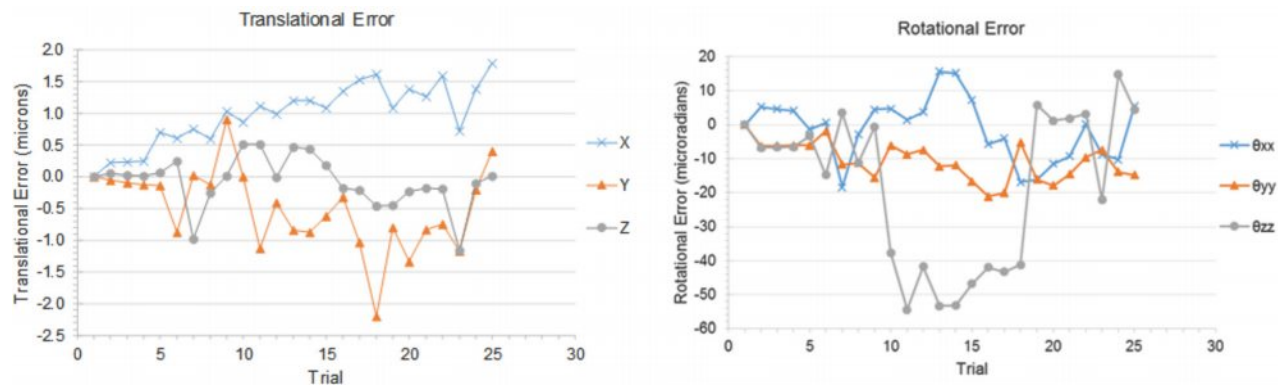


Fig. 11 (Left) Translational error versus (right) rotational error trial with outliers eliminated

Table 2 Standard deviation of wafer placement errors over 25 wafers

Error	$X (\mu\text{m})$	$Y (\mu\text{m})$	$Z (\mu\text{m})$	$\theta_x (\mu\text{rad})$	$\theta_y (\mu\text{rad})$	$\theta_z (\mu\text{rad})$
Total measured wafer loading system errors with outliers	2.085	3.54	7.464	84.9	99.4	24.0
Total measured wafer loading system errors without outliers	0.482	0.641	0.403	9.1	5.5	22.8
Measured kinematic coupling error	0.390	0.361	0.060	NA	NA	0.140
Estimated wafer only alignment error	0.283	0.530	0.398	9.1	5.5	22.8

wafer using the metrology frame, and σ_{KC} is the uncertainty in the kinematic coupling position

$$\sigma_{\text{Wafer}}^2 = \sigma_{\text{Measured}}^2 - \sigma_{\text{KC}}^2 \quad (8)$$

Using this correction, the estimated wafer alignment error is reduced to 283 nm in the x -direction, 530 nm in the y -direction, and 398 nm in the z -direction. The estimated rotational error does not change significantly since the rotational errors in the kinematic coupling are much lower than in the wafer loading system. Overall, these wafer loading repeatability values are a significant improvement compared to repeatability results from the manually loaded wafer alignment mechanism discussed in previous works [3,14] and the repeatability of the automated wafer loading system using passive alignment pins is adequate for many micro- and nano-manufacturing and metrology applications.

6 Discussion of Possible Improvements to the System

The low-cost automated wafer loading mechanism demonstrated submicron wafer positioning repeatability with throughput of approximately 60 wafers/h. A small percentage of loading trials (<10%) resulted in visibly misaligned wafers. These errors occurred when the side of the wafer made contact with the edge of the wafer cassette and the frequency of occurrence could be reduced by improving the fixturing and alignment of the wafer cassette relative to the robotic wafer handling platform. It is possible to detect these errors using a low-cost knife-edge sensing

system (approximate cost of less than \$200) and to correct for the errors by reloading the wafer. A diagram of the knife-edge sensing system is shown below in Fig. 12. The sensor consists of a laser diode positioned such that its beam is orthogonal to the top surface of a properly aligned wafer and approximately 50% of the beam is incident to the surface of the wafer. A photodetector aligned with the beam and fixed to the alignment stage below the wafer is used to measure positioning error as a function of intensity.

The current system wafer loading throughput is approximately 60 wafers/h. Throughput is limited by the control scheme, which uses a timer to wait a constant number of seconds between commands sent to the actuators. Eliminating the wait between commands could potentially increase throughput to approximately 120 wafers/h without significantly affecting the positioning repeatability. The wafer loading system currently runs in open-loop, which dictates the use of relatively slow travel rates in order to reduce positioning errors caused by system dynamics. Therefore, there is also potential to increase the rate of travel of each of the axes through the use of integrated sensing and closed-loop control in the current system. This would help to reduce the impact of system dynamics and allow the system to achieve faster response times. It is expected that with optimization of this controls system, load/unload times of less than 10 s could easily be achieved while still maintaining the submicron wafer alignment accuracy created by the passive alignment system. Therefore, through the use of improved system controls and optimization, it should be possible to achieve wafer throughputs of more than 300 wafers/h using this type of low-cost wafer alignment system.

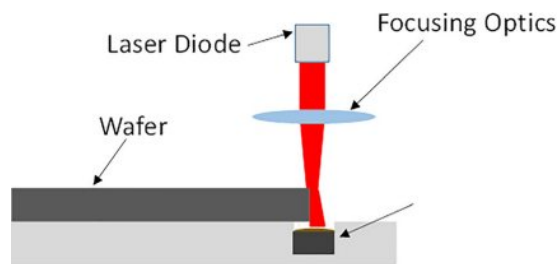


Fig. 12 Low-cost misalignment detector

7 Conclusions

This paper demonstrates how the use of a passive wafer alignment system in combination with a low-cost wafer handling robot can be used to achieve submicron wafer loading repeatability. This system was able to achieve a throughput of ~60 wafers/h with a wafer alignment loading repeatability of 283 nm in the x -direction, 530 nm in the y -direction, and 398 nm in the z -direction and an error rate of less than 10% at a cost of less than \$1800 for the entire system. Further improvements could be made to the system by implementing a knife-edge sensor to detect loading outliers and through the use of a closed-loop controls system

to improve wafer throughput. Overall, this low-cost, high accuracy wafer loading system is important for a number of nanomanufacturing and nanometrology applications where submicron alignment is necessary but market requirements prevent the use of an expensive wafer handling system. Therefore, the low-cost, high accuracy, high-throughput wafer alignment system presented in this paper could help to allow nanometrology platforms to be directly integrated into low-cost nanomanufacturing lines.

References

- [1] Zhang, M. T., and Goldberg, K., 2005, "Fixture-Based Industrial Robot Calibration for Silicon Wafer Handling," *Ind. Rob.: Int. J.*, **32**(1), pp. 43–48.
- [2] Mansour, R. R., Lee, G., Olfat, M., Strathearn, D., and Sarkar, N., 2015, "A 0.25 mm³ Atomic Force Microscope On-a-Chip," 2015 28th IEEE International Conference on Micro Electro Mechanical Systems (MEMS), Jan. 18–22, pp. 732–735.
- [3] Yao, T.-F., Duenner, A., and Cullinan, M. A., 2015, "In-Line, Wafer-Scale Inspection in Nano-Fabrication Systems," *ASPE* 2015 Annual Meeting, Austin, TX, Nov. 1–6, pp. 516–521.
- [4] Yao, T.-F., Duenner, A., and Cullinan, M. A., 2016, "In-Line Metrology of Nanoscale Features in Semiconductor Manufacturing Systems," *Precis. Eng.* (in press).
- [5] Mathia, K., 2010, *Robotics for Electronics Manufacturing: Principles and Applications in Cleanroom Automation*, Cambridge University Press, Cambridge, UK.
- [6] Brooks, 2012, "Atmospheric Robots" Spec Sheet, Brooks Automation, Chelmsford, MA, accessed Mar. 3, 2012, <http://www.brooks.com/products/semiconductor-automation/wafer-handling-robotics/atmospheric-robots>
- [7] Higuchi, M., Kawamura, T., Kaikogi, T., Murata, T., and Kawaguchi, M., 2003, "Mitsubishi Clean Room Robot-Clean Material Handling Originated from Plant Equipment Inspection," *Mitsubishi Juko Giho*, **40**(5), pp. 1–5.
- [8] Fuller, G. E., 2000, "Optical Lithography," *Handbook of Semiconductor Manufacturing Technology*, 2nd ed., R. Doering and Y. Nishi, eds., CRC Press, Boca Raton, FL, p. 469.
- [9] Marsh, A., 1984, "Wafer Alignment Performance Through an MOS Process," *Proc. SPIE*, **104**, pp. 104–110.
- [10] Uzawa, S., Suzuki, A., and Ayata, N., 1990, "New Alignment System for Submicron Stepper," *Proc. SPIE*, **1261**, pp. 325–331.
- [11] Li, N., Wu, W., and Chou, S. Y., 2006, "Sub-20-nm Alignment in Nanoimprint Lithography Using Moiré Fringe," *Nano Lett.*, **6**(11), pp. 2626–2629.
- [12] Slocum, A. H., and Weber, A. C., 2003, "Precision Passive Mechanical Alignment of Wafers," *J. Microelectromech. Syst.*, **12**(6), pp. 826–834.
- [13] Slocum, A. H., 1992, *Precision Machine Design*, Prentice-Hall, Eaglewood, NJ.
- [14] Duenner, A., and Cullinan, M. A., 2015, "Passive Semiconductor Wafer Alignment Mechanism to Support In-line Atomic Force Microscope Metrology," *ASPE* 2015 Annual Meeting, Austin, TX, Nov. 1–6.
- [15] Blanding, D. L., 1999, *Exact Constraint: Machine Design Using Kinematic Principles*, ASME Press, New York.
- [16] Norton, R. L., 2006, *Machine Design: An Integrated Approach*, Pearson, New York.